# An atomistic model for homogeneous melting

Sergio M. Davis,[1] Anatoly B. Belonoshko,[2] Börje Johansson,[1,3] and Anders Rosengren[2]

[1] *Applied Materials Physics, Department of Materials Science and Engineering, KTH, SE-100 44 Stockholm, Sweden*
[2] *Condensed Matter Theory, Department of Theoretical Physics, AlbaNova University Center, KTH, SE-106 91 Stockholm, Sweden*
[3] *Condensed Matter Theory Group, Department of Physics, Uppsala University, Uppsala Box 530, Sweden*

(Dated: August 31, 2009)

The diffusion statistics of atoms in a crystal close to the critical superheating temperature was studied in detail using molecular dynamics (MD) and Monte Carlo (MC) simulations. We present a general dynamic percolation model for diffusion of atoms hopping through thermal vacancies. The results obtained from our model suggest that the limit of superheating is precisely the temperature for which dynamic percolation happens at the time scale of a single individual jump. We show that this prediction of the critical superheating temperature can give an estimate of the melting point using only the dynamical properties of the solid state.

## I. INTRODUCTION

While it is a fairly common phenomenon in daily life, the complexity of melting at the atomic level is such that a precise physical explanation of its nature and, above all, its dynamics, is still lacking. Under special conditions, it is possible to overheat a solid (in an homogeneous way) above its melting point $T_m$, but there is a critical temperature, the limit of superheating $T_{LS}$, above which melting is unavoidable.

Besides the well-known Lindemann[1] criterion for melting, a number of additional criteria have been suggested, as an attempt to relate $T_{LS}$ with some qualitative change in the properties of the crystal. However, it seems that an irreversible nucleation of liquid precedes all of these[2,3], which therefore are no longer valid assumptions for explaining the triggering point of melting.

Recently it has been shown[4], using thermodynamic considerations, that this superheating limit is closely connected to the melting point itself, namely that the ratio $T_{LS}/T_m$ tends to $1 + \frac{1}{3}\ln 2$ at high pressures for monoatomic solids. Otherwise the origin and the nature of the superheating limit itself is far from clear. Previous studies using molecular dynamics (MD) have pointed out the importance of diffusion through thermal defects right at the limit of superheating[5–7], and it is known that the population of such defects sharply increases near this limit. But, can some qualitative change in the behavior of these thermal defects be ascribed as the meaning of $T_{LS}$?

In this paper we provide a random walk model which is able to explain the behavior of this kind of diffusion in a solid. Our model suggests that, in fact, the superheating limit is defined as the temperature at which the dynamic percolation threshold will be inevitably crossed.

## II. THE NEED FOR MICROCANONICAL SIMULATIONS OF SUPERHEATING: THE Z-METHOD

A recent approach to determine the melting point at high pressures using molecular dynamics is the Z-method[4], which does not require the simulation of coexistence between two phases. Instead, the idea is to perform micro–canonical (NVE) ensemble simulations on a single solid system at different temperatures in order to reach a realistic $T_{LS}$, without any external intervention on the dynamics of the melting process (due for example to "thermostat algorithms" used to constrain temperature). A system in the high pressure limit being simulated in the NVE ensemble slightly above $T_{LS}$ will melt, its temperature dropping naturally to $T_m$ at the pressure fixed by the chosen density.

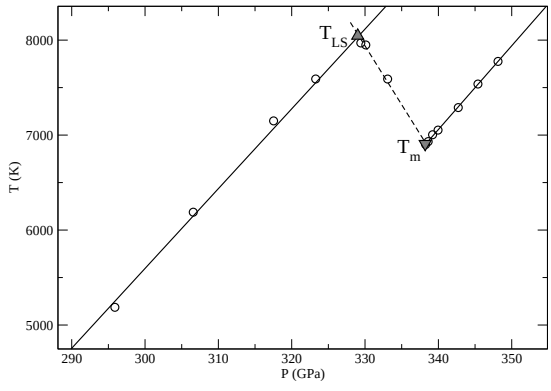


FIG. 1: Example of the application of the Z–method to determine the melting temperature. The relation between $T_m$ (lower point of the Z–shaped isochoric curve) and $T_{LS}$ (higher point) is shown for an embedded-atom solid.

At a fixed volume, the $(P, T)$ points of the isochoric

curve draw a "Z" shape (hence the name of the method), like the one shown in figure 1. In this "Z" shape the inflection at the higher temperature corresponds to $T_{LS}$ and the one at the lower temperature to $T_m$.

## III. MODEL FOR DIFFUSION

For the liquid state it is usual to compute the mean square displacement (MSD) of the atoms, as a function of time,

$$\left\langle r(\tau)^2 \right\rangle = \left\langle (\vec{r}(t_o+\tau) - \vec{r}(t_o))^2 \right\rangle, \tag{1}$$

where the average in the right-hand side is taken over all atoms and all origins of time $t_o$. In a liquid the MSD is linear with time, and the diffusion coefficient comes directly from

$$\left\langle r(\tau)^2 \right\rangle = 2dD \cdot \tau, \tag{2}$$

where $d$ is the dimensionality of the system.

The analysis of the MSD is useful to get an overall view of the diffusive properties of the system, but it does not give any details about the diffusivity of individual atoms, or the statistical distribution behind the MSD average.

For this purpose we can define the probability distribution of displacements $J(r,\tau)$, as the number of atoms travelling a distance between $r$ and $r+\Delta r$ in a time interval $\tau$. The MSD can be obtained as the expectation value of $r^2$ under the probability distribution $J$, i.e.,

$$\left\langle r(\tau)^2 \right\rangle = E_J\left(r^2\right) = \int_0^\infty r^2 J(r,\tau) dr. \tag{3}$$

For the sake of brevity we shall refer to the function $J(r)$ (i.e. $J(r,\tau)$ taken at a constant $\tau$) as the mobility histogram of the system for the given observation interval $\tau$. An example of such a histogram for two different temperatures in a solid close to $T_{LS}$=8000 K is shown in figure 2. Note the decrease of the first peak ($r/r_0 < 0.5$) and the corresponding increase of the second ($0.5 < r/r_0 < 1.5$) and third ($r/r_0 > 1.5$) peaks when increasing temperature.

Considering a fixed observation interval $\tau$ we can roughly classify the population of atoms into three kinds: atoms with displacement around zero, atoms with displacement around the nearest neighbor distance $r_0$, and atoms with displacement larger than $r_0$. These three kinds of atoms will have fractional populations $J_0$, $J_1$ and $J_r$, such that

$$J_0 + J_1 + J_r = 1, \tag{4}$$

These fractional populations (or mobility components) can be obtained from $J(r,\tau)$ by taking the integral over $r$,

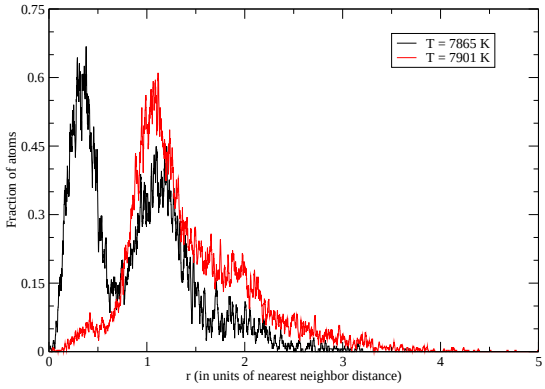


FIG. 2: Mobility histograms $J_\tau(r)$ obtained from molecular dynamics simulations of an embedded atom solid close to $T_{LS}$.

$$J_0(\tau) = \frac{1}{N}\int_0^{\rho_0} J(r,\tau) dr \tag{5}$$

$$J_1(\tau) = \frac{1}{N}\int_{\rho_0}^{\rho_1} J(r,\tau) dr \tag{6}$$

$$J_r(\tau) = \frac{1}{N}\int_{\rho_1}^{\infty} J(r,\tau) dr. \tag{7}$$

where $\rho_0$ is taken as the minimum distance between atoms (due to repulsion) and $\rho_1$ is taken as slightly higher than $r_0$, in order to include the whole first-neighbor shell. In practice both radii can be obtained from the radial distribution function (RDF).

For an ideal solid without defects, the only displacement of the atoms is due to thermal vibrations around their equilibrium positions. In this case, $J_0(\tau) = 1$. If we consider thermal defects, depending on the observation time $\tau$, some atoms will jump to the nearest vacant site, or even jump further away through a series of jumps. Those "diffusive" atoms will contribute to $J_1$ and $J_r$ at the expense of decreasing $J_0$, the fraction of "non–diffusive" atoms.

Taking this into account, it is clear that the mobility histogram (and its components $J_0$, $J_1$ and $J_r$) will be highly dependent on the number of vacant sites $f$ available to jump, which in the case of a finite-temperature crystal corresponds to the equilibrium fraction of thermal vacancies[8],

$$f = e^{-E_v/k_B T}, \tag{8}$$

where $E_v$ is the energy needed to create a vacancy–insterstitial pair in the crystal.

It will also be dependent on the average number of successful jumps $n_j$ performed during the time interval

$\tau$. This in turn is given by the probability of jumping $P_j$, as $n_j$=$P_j(\tau/\tau_j)$, where $\tau_j$ is the average time it takes an atom to jump.

In a finite-temperature crystal $P_j$ is also given by a Boltzmann factor,

$$P_j = e^{-E_j/k_B T}, \tag{9}$$

where $E_j$ is the energy barrier the atom has to cross in order to jump into a neighboring vacant site.

If we consider the effects of temperature only through $f(T)$ and $P_j(T)$ we can reduce the problem of studying the statistics of diffusion in a crystal with defects to a discrete mathematical problem of random walk over a percolation lattice[9].

## IV. MATHEMATICAL DESCRIPTION OF THE RANDOM WALK ON A LATTICE

The simpler problem of an isotropic random walk over a lattice is fully described by the probability of reaching a given lattice point $\vec{r}$, starting from the origin, in $n$ steps. This probability, denoted as $P_n(\vec{r})$, can be obtained from the ordinary generating function

$$P(\vec{r}; z) = \sum_{n=0}^{\infty} P_n(\vec{r}) z^n, \tag{10}$$

called the lattice Green's function at the lattice point $\vec{r}$. For a given lattice, $P(\vec{r}; z)$ can be computed as[9]

$$P(\vec{r}; z) = \frac{1}{(2\pi)^d} \int_B \frac{e^{-i\vec{k}\cdot\vec{r}}}{1 - \tau\lambda(\vec{k})} d\vec{k} \tag{11}$$

where $\lambda(\vec{k})$ is the structure function for the lattice, and the integration is performed over the first Brillouin zone, $d$ being the dimensionality of the lattice.

The structure function $\lambda(\vec{k})$ includes the probability of jumping to the different sites from the origin, and is defined as

$$\lambda(\vec{k}) = \sum_i e^{i\vec{k}\cdot\vec{R}_i} p(\vec{R}_i), \tag{12}$$

where the summation is performed over all the allowed jump displacements $\vec{R}_i$ from the origin, and $p(\vec{r})$ is the probability associated to the displacement $\vec{r}$.

If we assume the jump events follow a Poisson distribution in time, with the average number of jumps in a time interval $\tau$ given by

$$\langle n(\tau) \rangle = \frac{P_j \tau}{\tau_j}, \tag{13}$$

we can obtain a model for a continuous-time random walk on a lattice, which will be characterized by the Poisson generating function

$$G(\vec{r}; \tau) = \sum_{n=0}^{\infty} P_n(\vec{r}) \frac{(P_j\tau/\tau_j)^n}{n!} e^{-P_j\tau/\tau_j}. \tag{14}$$

This function gives directly the probability of reaching a lattice point $\vec{r}$ from the origin in a time interval $\tau$. If we include equations 10 and 11, we have

$$G(\vec{r}; \tau) = \frac{e^{-P_j\tau/\tau_j}}{(2\pi)^d} \int_B e^{-i\vec{k}\cdot\vec{r} + (P_j\tau/\tau_j)\lambda(\vec{k})} d\vec{k}. \tag{15}$$

From $G(\vec{r}; \tau)$ we can obtain the mobility components as

$$J_0(\tau) = G(\vec{0}; \tau) \tag{16}$$

$$J_1(\tau) = \frac{1}{n_c} \sum_i G(\vec{R}_i; \tau) \tag{17}$$

$$J_r(\tau) = 1 - J_0(\tau) - J_1(\tau). \tag{18}$$

with $n_c$ the coordination number of the lattice. For the simple case of the square lattice, equation 15 can be evaluated exactly at the origin and over the first neighbors. Then $J_0$ and $J_1$ can be obtained as

$$J_0(\tau) = e^{-P_j\tau/\tau_j} I_0^2\left(\frac{P_j\tau}{2\tau_j}\right) \tag{19}$$

$$J_1(\tau) = 4e^{-P_j\tau/\tau_j} I_0\left(\frac{P_j\tau}{2\tau_j}\right) I_1\left(\frac{P_j\tau}{2\tau_j}\right) \tag{20}$$

where the $I_k(x)$ are the modified Bessel functions of the first kind.

Figure 3 shows the mobility components obtained from MC simulations of the isotropic random walk in a square lattice, compared to the exact solutions (equations 19 and 20).

A perfect agreement which validates the MC simulations and the assumption of Poisson statistics for the jump events.

These mobility curves can be interpreted as follows: increasing the observation interval $\tau$ leads to a monotonic decrease in the population of non-diffusive atoms ($J_0$), together with an, also monotonic, increase in the population of long-range diffusive atoms ($J_r$). However $J_1$, the population of atoms sitting one nearest-neighbor distance from their equilibrium positions, reaches a maximum value $J_c$ and then decreases. This marks out two regimes, one where the atoms mainly hop following closed paths, quickly returning to their starting positions (recurrent random walk states), and another where the atoms

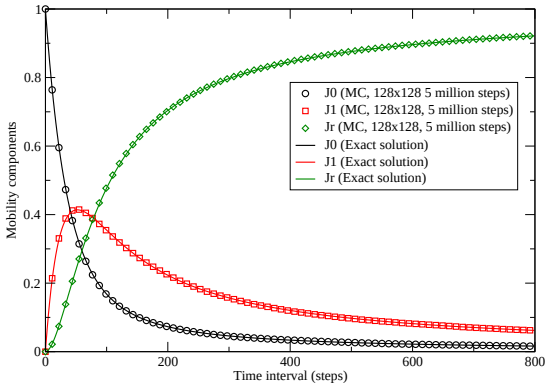


FIG. 3: Mobility components for the simple random walk in a square lattice.

wander far away following open paths, eventually percolating through the entire system if the observation interval is large enough (transient random walk states)[9,10].

From the curves in figure 3 we can define two characteristic observation intervals, or *crossing times*, $\tau_0$ and $\tau_1$, such that

$$J_0(\tau_0) = J_r(\tau_0) \quad (21)$$
$$J_0(\tau_1) = J_1(\tau_1). \quad (22)$$

The crossing time $\tau_1$ is the average time interval needed to observe a single jump. It only depends on the frequency of attempts to jump $\tau_j^{-1}$ and the probability of jumping $P_j$. The crossing time $\tau_0$ is the average time interval needed to jump beyond the first-neighbor shell. So, for $\tau < \tau_1$ the atoms are just oscillating around their equilibrium positions, for $\tau_1 < \tau < \tau_0$ the atoms are mostly jumping back and forth, and for $\tau > \tau_0$ the atoms are diffusing away from their starting positions.

## V. MONTE CARLO SIMULATIONS

The presence of vacancies mediating the jumps can be included by modifying the structure function $\lambda(\vec{k})$ to include a finite probability to jump, which will depend on the availability of vacancies around the starting point,

$$\lambda'(\vec{k}; f) = \sum_i e^{i\vec{k}\cdot\vec{R}_i} F(f; n_c) p(\vec{R}_i) = F(f; n_c)\lambda(\vec{k}), \quad (23)$$

where $F(f; n_c)=(1 - e^{-f n_c})$ is the probability of having at least one available neighbor vacancy to jump into.

In this way, the new Poisson generating function $G(\vec{r}; \tau, f)$ can be expressed as

$$G(\vec{r}; \tau, f) = \frac{e^{-P_j\tau/\tau_j}}{(2\pi)^d} \int_B e^{-i\vec{k}\cdot\vec{r} + \frac{P_j\tau F(f;n_c)}{\tau_j}\lambda(\vec{k})} d\vec{k}. \quad (24)$$

and the mobility components as simple corrections over equations 19 and 20,

$$J_0(\tau; f) = e^{-P_j\tau/\tau_j} I_0^2\left(\frac{P_j\tau F(f; n_c)}{2\tau_j}\right) \quad (25)$$

$$J_1(\tau; f) = n_c e^{-P_j\tau/\tau_j} I_0\left(\frac{P_j\tau F(f; n_c)}{2\tau_j}\right) I_1\left(\frac{P_j\tau F(f; n_c)}{2\tau_j}\right). \quad (26)$$

In order to confirm the validity of this expression we performed MC simulations of the discrete vacancy-driven random walk on a lattice.

In this approach, the system consists of a lattice of $N$ points, where initially every point has a probability $f$ of being an empty site (a vacancy) and $1 - f$ of being an occupied site (an atom).

For the Markov chain, the move consists simply of attempting to exchange a vacancy with an occupied site, with probability $P_j$. In this way, the total number of vacancies $Nf$ is kept constant during the simulation.

Figure 4 plots equations 25 and 26 against the results from MC simulations of the square lattice. There is an overall agreement, except for small deviations around the maximum of $J_1$, precisely the region where dynamic percolation is expected.

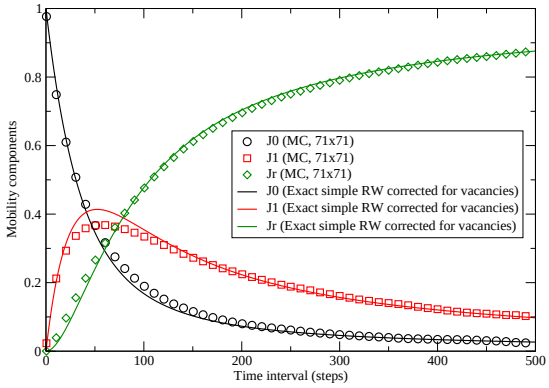


FIG. 4: Mobility components for the vacancy-mediated random walk in a square lattice.

Due to the complexity of the exact mathematical expressions for the vacancy-mediated random walk problem, we have studied several crystal structures via MC simulations. Following the same procedure used for the square lattice, we computed the mobility components for

different values of $f$ and $P_j$ as a function of the observation time $\tau$, and fitted them to generalized logistic curves. The generalized logistic curve has the form

$$L(x;Q,\alpha,\nu) = \left(1 + Qx^{-\alpha\nu}\right)^{-1/\nu}. \tag{27}$$

From these simulations we confirmed that $J_0$, $J_1$ and $J_r$ are, in all cases, universal functions of both $\tau$ and $f$. Keeping $f$ constant there is a maximum in $J_1$ at $\tau = \tau_c(f)$, and, conversely, keeping $\tau$ constant there is a maximum in $J_1$ at $f = f_c(\tau)$. The value of $f_c(\tau)$ follows a power law,

$$f_c(\tau) = \frac{n_j^{-b}}{K}, \tag{28}$$

where $K$ and $b$ depend on the crystal structure, their values are shown in table I.

| Structure | $K$ | $b$ |
|---|---|---|
| SC | 0.851 | 0.870 |
| BCC | 1.154 | 0.814 |
| FCC | 1.110 | 0.814 |
| HCP | 0.845 | 0.900 |
| Honeycomb | 0.804 | 0.711 |
| Square | 0.776 | 0.791 |
| Hexagonal | 0.955 | 0.748 |

TABLE I: Parameters $K$ and $b$ for the different 3D and 2D lattices.

Using the new variables $f'=f/f_c$ and $\tau'=\tau/\tau_c$, the mobility components look as shown in figure 5.

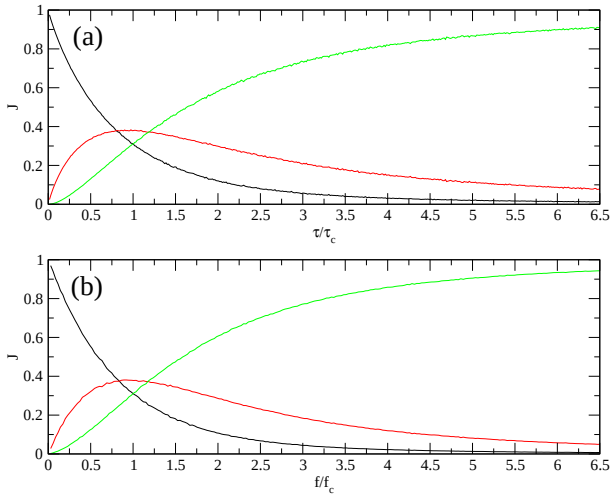


FIG. 5: Mobility components $J_0$, $J_1$ and $J_r$ as a function of the normalized variables $f'$ and $\tau'$ for the case of BCC structure.

We find that two of the mobility components $J_0$ and $J_r$, can be fitted to

$$J_0(z) = 1 - L(z;Q_0,\alpha_0,\nu_0) \tag{29}$$

$$J_r(z) = L(z;Q_r,\alpha_r,\nu_r) \tag{30}$$

Tables II and III show the values of the parameters, obtained from MC simulations, for three-dimensional and two-dimensional lattices, respectively.

| Structure | $n_c$ | $\alpha_0$ | $\alpha_r$ | $\nu_0$ | $\nu_r$ | $J_c$ |
|---|---|---|---|---|---|---|
| SC | 6 | 0.735324 | 1.47825 | 2.62313 | 1.16798 | 0.38385 |
| BCC | 8 | 0.740585 | 1.51783 | 2.76984 | 1.12153 | 0.38645 |
| FCC | 12 | 0.751794 | 1.59069 | 2.79555 | 1.07426 | 0.46082 |
| HCP | 12 | 0.759472 | 1.59175 | 2.72982 | 1.06805 | 0.45791 |

TABLE II: Generalized logistic curve parameters for several 3D lattices, obtained from MC simulations.

| Structure | $n_c$ | $\alpha_0$ | $\alpha_r$ | $\nu_0$ | $\nu_r$ | $J_c$ |
|---|---|---|---|---|---|---|
| Honeycomb | 3 | 0.662424 | 1.396345 | 2.0141 | 0.923805 | 0.38738 |
| Square | 4 | 0.705221 | 1.50258 | 2.04747 | 0.805146 | 0.37771 |
| Hexagonal | 6 | 0.75522 | 1.60351 | 2.00981 | 0.791778 | 0.46132 |

TABLE III: Generalized logistic curve parameters for several 2D lattices, obtained from MC simulations.

It is interesting to note that $J_c$ seems to have only two possible values: either close to 0.46 for the close-packed structures (FCC and HCP structures in 3D, hexagonal structure in 2D) or close to 0.38 for the loose-packed ones.

The explanation for this discrete behavior of $J_c$ could be related to the enumeration of closed jump paths[9] implicit in $P_n(\vec{0})$. For a loose-packed structure, there is no closed graph on the lattice with an odd number of edges. However, for a closed-packed structure there are closed graphs with odd and even number of edges. The number of closed graphs is directly related to $J_0(\tau)$ and also indirectly to $J_1(\tau)$, because every $n$-step random walk trajectory contributing to $J_1$ can be mapped to a $(n+1)$-step closed trajectory (by adding the edge that closes the loop).

In order to see that our discrete-jump model captures the essence of the dynamics of the crystal, we compare the mobility components for MC simulations of an ideal FCC structure with molecular dynamics simulations of a Lennard-Jones solid. The results are shown in figure 6.

In terms of the finite-temperature crystal, as temperature increases both $f$ and $P_j$ will increase as well, according to equations 8 and 9. Eventually the concentration of thermal defects and the rate of barrier crossing events will be high enough that the system will cross its dynamic percolation threshold $\tau_0$, the population $J_r$ overcoming

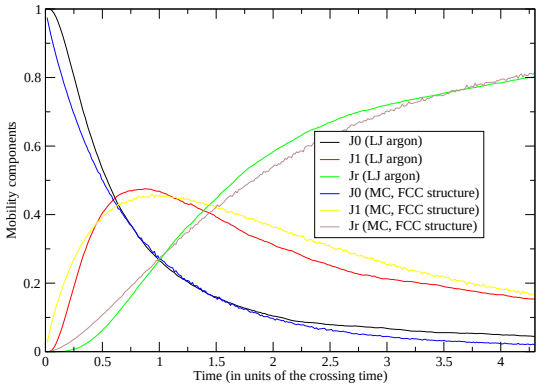


FIG. 6: Comparison between the $J_i$ curves as a function of observation time for Lennard-Jones MD (Ar, 108 atoms) and the MC geometrical model.

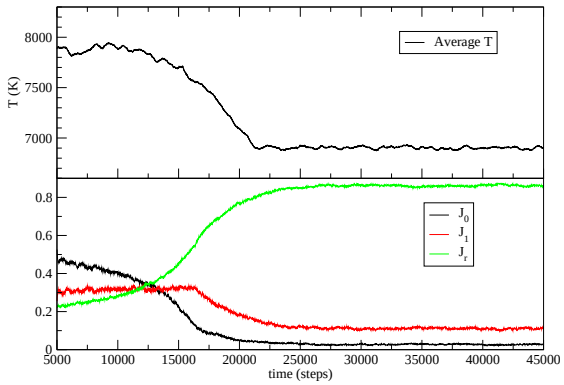


FIG. 7: (a) Instantaneous temperature as a function of time during melting. (b) Jump diffusion components as a function of time.

$J_0$. Given that the spatial distribution of vacancies and atoms changes over time, it is possible to achieve percolation even when the concentration of vacancies is less than the "static" site percolation threshold[11].

From this moment on, after the first jump occurs the atoms will diffuse in a similar way as a non-restricted random-walk over the points of the lattice. In this metastable state the mean square displacement follows a power law,

$$\left\langle r^2(\tau)\right\rangle \propto \tau^{\gamma} \tag{31}$$

To study the connection of this kind of diffusion with the superheating limit, we have computed the temporal evolution of $J_0$, $J_1$ and $J_r$, as well as the exponent $\gamma$, during several MD simulations at increasing temperatures, near $T_{LS}$. The mobility components are shown in figure 7 for the case when the crystal melts, and figure 8 shows the thermal dependence of $\gamma$.

We can see that, according to the drop in instantaneous temperature, the instant when melting is triggered corresponds precisely to the crossing of $J_0$ and $J_r$. This is valid for every observation interval $\tau$ large enough to see contributions to $J_1$.

## VI. TWO-DIMENSIONAL SIMULATIONS OF SUPERHEATING

In order to see any similarities of the melting mechanism in two and three dimensions, we performed molecular dynamics simulations of a two-dimensional system. We studied melting of the triangular lattice, the interatomic interaction being described by the Lennard-Jones potential with the usual argon parameters. This is the

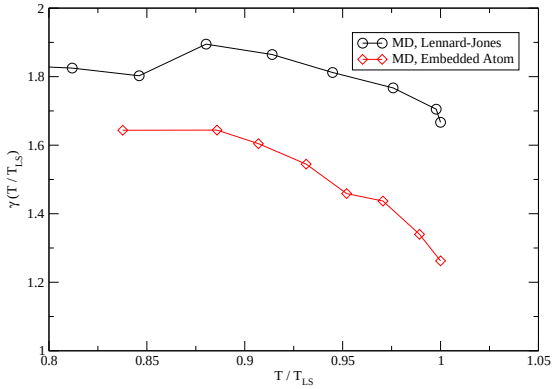


FIG. 8: Mean square displacement exponent $\gamma$ as a function of temperature for the LJ and EAM solids.

same model we have employed in our studies of the melting mechanism in three dimensions[4,7].

The density was chosen in such a way so that the system will be slightly compressed. That is, the first neighbors are located at a distance about 3.2 Å, which is slightly smaller than the Lennard-Jones $\sigma$ parameter, 3.405 Å. Each $(P, T)$ point in figure 9 was again obtained following the Z-method. We studied three different system sizes - 30x30, 40x40, and 60x60 atoms. We can see that, starting at $T$ around 160 K (the exact value will depend on the system size) the curves' behavior becomes irregular. It is especially evident for the smallest system, and rather smooth for the largest system. In this range of pressure and temperature we notice the formation of interfaces in the system. As percolation starts to

be favorable, extended defects are formed. This of course requires energy, and the isochoric curves exhibit plateaus - some kinetic energy is spent on the formation of each extended defect. Apparently, the size of the plateau depends on the ratio between the linear size of the defect to the total energy, that is the total number of atoms in the system. In other words, it changes as $1/N$. Of course, the effect is not quite linear. Thus, melting in 2D is the process of fracturing the lattice by percolating extended defects. This can also explain why the transition is continuous (second order), unlike the three-dimensional case, i.e., why there is no clear superheating limit $T_{LS}$ in two-dimensions. As soon as the 2D lattice is percolated, the divided parts become the same non-percolated crystals and the process of percolation has to be repeated for the smaller parts.

The system melts when the size of a non-percolated region becomes comparable to the atomic size. At this point, the system can be considered as a liquid, because all the atoms become equally mobile. This is different from the 3D case, where the formation of a percolating defect does not separate the 3D system in two, but rather radically changes the 3D system - the channel for diffusion becomes available within the system. Such diffusion eventually leads to complete melting.

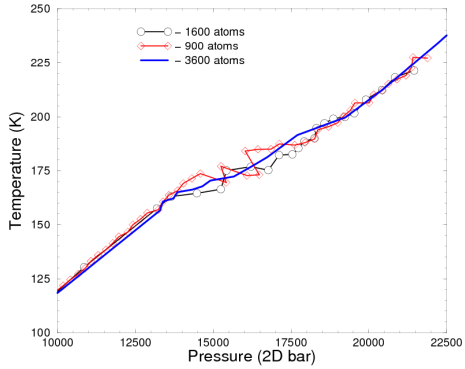


FIG. 9: $P$-$T$ isochoric curves from Z-method simulations on a two-dimensional Lennard-Jones system.

## VII. CONNECTION BETWEEN $T_{LS}$ AND THE MOBILITY COMPONENTS

From MD simulations at $T_{LS}$ we note that the mobility curves $J_0$, $J_1$ and $J_r$ always seem to cross at the same time interval $\tau_D$=$\tau_0$=$\tau_1$, whereas for $T$ above or below $T_{LS}$ there is a clear separation between the different diffusion time scales $\tau_0$ and $\tau_1$. This is shown in figure 10.

The behavior of $\tau_0$ and $\tau_1$ with increasing temperature is shown in figure 11. It is clear that, as one approaches $T_{LS}$, not only does $\tau_0$ decrease, but it becomes closer and closer to $\tau_1$. Eventually at $T$=$T_{LS}$ we have $\tau_0$=$\tau_1$=$\tau_D$, and then

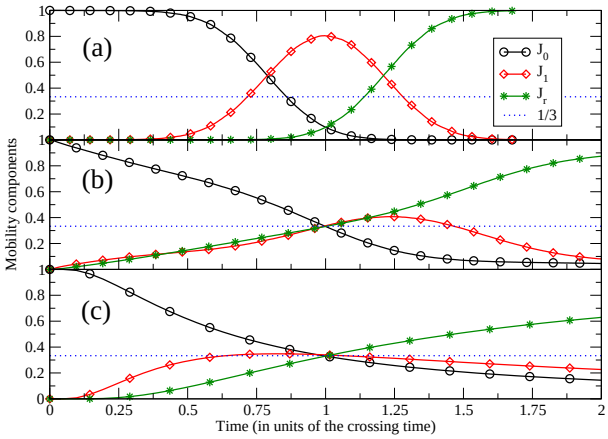


FIG. 10: Mobility components computed from MD simulations as a function of the normalized observation time $\tau/\tau_0$, (a) at $T < T_{LS}$ in the solid isochore, (b) at $T_{LS}$ and, (c) in the liquid isochore. The dotted line, J=1/3 is drawn for clarity.

$$\langle J_0(\tau_D)\rangle_{LS} = \langle J_1(\tau_D)\rangle_{LS} = \langle J_r(\tau_D)\rangle_{LS} = \frac{1}{3} \qquad (32)$$

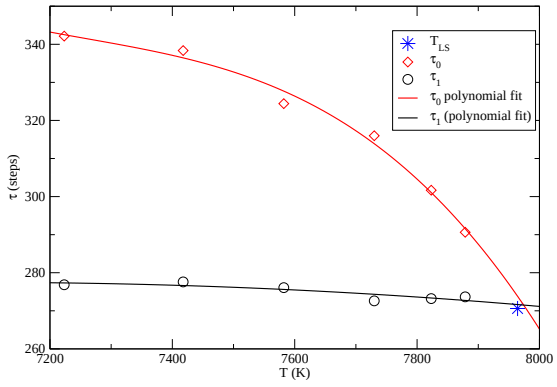


FIG. 11: Characteristic observation times $\tau_0$ and $\tau_1$ on increasing temperatures, close to $T_{LS}$. The star corresponds to the measured $T_{LS}$ and $\tau$=$\tau_D$.

This "collapse" of the three $J_i$ curves to 1/3 does not arise from our simple geometric MC model, as in this model the positions on the crystal lattice are fixed, only exchanges between atoms and vacancies are allowed as moves in the Markov chain process. In that case $J_c = J_1(\tau_0)$ is always close to either 0.38 (for loose-packed

structures) or 0.45 (for close-packed ones). We know from the MC model that $J_c$ is directly related to the distribution of closed random walk paths, therefore the fact that $J_c$ tends to 1/3 at $T_{LS}$ in MD simulations seems to suggest that the crystal becomes even less packed (in terms of the possible closed trajectories) than the original structure just prior to melting.

| System | $T_{LS}$ (K) | $\tau_j$ (fs) | $n_D$ | $S_D$ ($k_B$) | $\epsilon$ (eV) |
|---|---|---|---|---|---|
| Fe, BCC, 130 GPa | 4543 | 37.5 | 800 | 5.585 | 2.186 |
| Ar, FCC, 60 GPa | 6014 | 40 | 926 | 5.665 | 2.936 |
| Fe, BCC, 330 GPa | 7964 | 25 | 544 | 5.271 | 3.617 |
| Fe, HCP, 330 GPa | 8577 | 27 | 4445 | 7.391 | 5.463 |

TABLE IV: The characteristic number of periods of observation $n_D$ and the combined energy of vacancy and jump $\epsilon$ for different simulated systems and conditions.

Following this empirical observation, if we now assume that $T_{LS}$ is defined as the temperature where $\tau_0 = \tau_D$, we can define $T_{LS}$ as a function of the energy of formation of vacancies $E_v$ and the height of the energy barrier $E_j$, through $f$ and $P_j$. Let's define the mobility parameter $z = f/f_c$ so that $z = 1$ marks the crossing point between $J_0$ and $J_r$. Then $z$ will depend on $f$ and $P_j$ as

$$z(f, P_j, \tau) = f/f_c(\tau) = Kf \left( \frac{P_j \tau}{\tau_j} \right)^b . \qquad (33)$$

Changing the dependence on $f$ and $P_j$ in favor of a single dependence on $T$, we have

$$z(T, \tau) = K \left( \frac{\tau}{\tau_j} \right)^b e^{-\frac{E_v + bE_j}{k_B T}} \qquad (34)$$

As $\tau_D = \tau_0$ at $T_{LS}$, $z(T_{LS}, \tau_D)$=1, and then

$$K \left( \frac{\tau_D}{\tau_j} \right)^b e^{-(E_v + bE_j)/k_B T_{LS}} = 1 \qquad (35)$$

From which follows that,

$$T_{LS} = \frac{\epsilon}{k_B \ln(K n_D^b)}, \qquad (36)$$

where $n_D$=$\tau_D/\tau_j$ is a characteristic time scale, measured in terms of number of atomic oscillations, and $\epsilon$=$E_v$+$bE_j$ is an energy which is material-dependent, as shown in table IV.

## VIII. CONCLUSIONS

We have developed and tested a model to explain jump-mediated diffusion due to thermal vacancies near $T_{LS}$ and its role in defining it. The application of our model to MD simulations suggests that $T_{LS}$ is the temperature at which the change in diffusion behavior, from recurrent random walks to transient random walks, takes place at a particular time scale $\tau_D$, which can be determined from analysis of the mobility of the solid phase.

## IX. ACKNOWLEDGEMENTS

Computations were performed at the National Supercomputer Center (NSC) in Linköping and the Parallel Computer Center (PDC) in Stockholm. We also thank the Swedish Research Council VR for financial support.

[1] F. A. Lindemann, Z. Phys. Chem., Stoechiom. Verwandtschaftsl. **11**, 609 (1910).
[2] K. Lu and Y. Li, Phys. Rev. Lett. **80**, 4474 (1998).
[3] Z. H. Jin, P. Gumbsch, K. Lu, and E. Ma, Phys. Rev. Lett. **87**, 055703 (2001).
[4] A. B. Belonoshko, N. V. Skorodumova, A. Rosengren, and B. Johansson, Phys. Rev. B **73**, 012201 (2006).
[5] M. Forsblom and G. Grimvall, Nature Materials **4**, 388 (2005).
[6] M. Forsblom and G. Grimvall, Phys. Rev. B **72**, 054107 (2005).
[7] A. B. Belonoshko, S. Davis, N. V. Skorodumova, P. H. Lundow, A. Rosengren, and B. Johansson, Phys. Rev. B **76**, 064121 (2007).
[8] M. Hillert, *Phase equilibria, Phase Diagrams and Phase Transformations* (Cambridge University Press, 1998).
[9] B. D. Hughes, *Random Walks and Random Environments* (Clarendon Press, Oxford, 1995).
[10] F. Spitzer, *Principles of Random Walk* (D. Van Nostrand Company, 1964).
[11] G. Grimmett, *Percolation* (Springer-Verlag, 1989).